AFRL-RQ-WP-TR-2020-0040

SPALL PROPAGATION CHARACTERISTICS OF LIFE-TESTED, VACUUM-INDUCTION-MELTED, VACUUM-ARC RE-MELTED (VIM-VAR) M50 AND PYROWEAR 675 BEARING STEELS

Lewis Rosado, Ph.D. and Mathew S. Kirsch, Ph.D.

Engine Mechanical Systems Branch
Turbine Engine Division

Hitesh K. Trivedi and DaMari A. Haywood

UES, Inc.

APRIL 2020
Final Report

AIR FORCE RESEARCH LABORATORY
AEROSPACE SYSTEMS DIRECTORATE
WRIGHT-PATTERSON AIR FORCE BASE, OH 45433-7542
AIR FORCE MATERIEL COMMAND
UNITED STATES AIR FORCE

NOTICE AND SIGNATURE PAGE

This report was cleared for public release by the USAF 88th Air Base Wing (88 ABW) Public Affairs Office (PAO) and is available to the general public, including foreign nationals.

Copies may be obtained from the Defense Technical Information Center (DTIC) (https://discover.dtic.mil/).

AFRL-RQ-WP-TR-2020-0040 HAS BEEN REVIEWED AND IS APPROVED FOR PUBLICATION IN ACCORDANCE WITH ASSIGNED DISTRIBUTION STATEMENT.

REPORT DOCUMENTATION PAGE

Form Approved
OMB No. 0704-0188

1. REPORT DATE *(DD-MM-YY)*	2. REPORT TYPE	3. DATES COVERED *(From - To)*
April 2020	Final	1 August 2018 – 1 December 2019

4. TITLE AND SUBTITLE

SPALL PROPAGATION CHARACTERISTICS OF LIFE-TESTED, VACUUM-INDUCTION-MELTED, VACUUM-ARC RE-MELTED (VIM-VAR) M50 AND PYROWEAR 675 BEARING STEELS

5a. CONTRACT NUMBER
In-house

5b. GRANT NUMBER

5c. PROGRAM ELEMENT NUMBER
62203F

6. AUTHOR(S)

Lewis Rosado, Ph.D. and Mathew S. Kirsch, Ph.D. (AFRL/RQTM)
Hitesh K. Trivedi and DaMari A. Haywood (UES, Inc.)

5d. PROJECT NUMBER
3048

5e. TASK NUMBER

5f. WORK UNIT NUMBER
Q0S6

7. PERFORMING ORGANIZATION NAME(S) AND ADDRESS(ES)

Engine Mechanical Systems Branch (AFRL/RQTM)
Turbine Engine Division
Air Force Research Laboratory Aerospace Systems Directorate
Wright-Patterson Air Force Base, OH 45433-7542
Air Force Materiel Command, United States Air Force

UES, Inc.
4401 Dayton-Xenia Road
Dayton, OH 45432

8. PERFORMING ORGANIZATION REPORT NUMBER
AFRL-RQ-WP-TR-2020-0040

9. SPONSORING/MONITORING AGENCY NAME(S) AND ADDRESS(ES)

Air Force Research Laboratory
Aerospace Systems Directorate
Wright-Patterson Air Force Base, OH 45433-7542
Air Force Materiel Command
United States Air Force

10. SPONSORING/MONITORING AGENCY ACRONYM(S)
AFRL/RQTM

11. SPONSORING/MONITORING AGENCY REPORT NUMBER(S)
AFRL-RQ-WP-TR-2020-0040

12. DISTRIBUTION/AVAILABILITY STATEMENT

DISTRIBUTION STATEMENT A. Approved for public release. Distribution is unlimited.

13. SUPPLEMENTARY NOTES

PA Clearance Number: 88ABW-2019-2047; Clearance Date: 17 April 2019.

14. ABSTRACT

Spall propagation experiments were conducted on fatigue life-tested 208-size angular contact bearings made of vacuum induction melted, vacuum arc re-melted (VIM-VAR) M50 (with both M50 and Si_3N_4 rolling elements) and two heat treatment variations of VIM-VAR Pyrowear 675 (P675) (with Si_3N_4 rolling elements). The primary focus was to study the effect of accumulated stress cycles and spall initiation method on spall propagation rate. Bearings were initially tested for rolling contact fatigue (RCF) life at maximum Hertzian contact stress values of 3.10 GPa (all-metal) and 3.56 GPa (hybrid) and at a temperature of 128 °C using high thermal stability (HTS) oil conforming to MIL-PRF-23699F. Spall propagation tests were then subsequently conducted on fatigue life-tested bearings at 2.41 GPa (350 ksi) maximum Hertzian contact stress until a pre-determined amount of material removal was detected. Propagation experiments were performed on both naturally occurring fatigue spalls from life testing and spalls initiated from Rockwell hardness indentations on suspended life-tested bearings. Selected life-tested bearings were investigated for alteration in microstructure and residual stress prior to spall propagation experiments. The effect of alloy, heat treatment and stress cycling on spall propagation rate was examined. The material microstructural decay from accumulated stress cycles had a significant effect on spall propagation time of hybrid bearings.

15. SUBJECT TERMS

turbine engine, bearing, spall propagation, steel

16. SECURITY CLASSIFICATION OF:			17. LIMITATION OF ABSTRACT:	18. NUMBER OF PAGES	19a. NAME OF RESPONSIBLE PERSON (Monitor)
a. REPORT	b. ABSTRACT	c. THIS PAGE			Brian D. Nicholson
Unclassified	Unclassified	Unclassified	SAR	30	19b. TELEPHONE NUMBER (Include Area Code) N/A

TABLE OF CONTENTS

LIST OF FIGURES

LIST OF TABLES

ACKNOWLEDGEMENTS

This research was funded by the Air Force Research Laboratory (AFRL) and performed at the Engine Mechanical Systems Branch, Turbine Engine Division, Aerospace Systems Directorate, Wright-Patterson AFB and conducted, in part, under U.S. Air Force Contract No. FA8650-14-D-2348. The authors would like to acknowledge the support of David Gerardi and Doug Eisentraut, UES, Inc. for experimental work, Jan Clark, UES, Inc. for manuscript preparation, Bryan McCoy and Eric Youngquist, SKF Aeroengine North America for providing bearing test assets, Garry Givan (retired, AFRL) and Kevin Thompson, AFRL, for program management oversight and Nelson Forster (retired, AFRL) for the notion and guidance of using the oil debris monitor (ODM) for real-time tracking of spall propagation characteristics of advanced bearing materials via seeded fault experimentation.

1 INTRODUCTION

Bearings are a critical component of aerospace gas turbine engines. A catastrophic bearing failure can lead to a loss of aircraft and loss of life. This is a major safety concern for single engine aircraft in which the mainshaft bearings are operating at high speed, load and temperature conditions. For rolling contact fatigue life calculations, a bearing is considered failed at the initiation of a fatigue spall. A very small amount (few milligrams) of material is removed from the bearing at spall initiation. If the bearing is allowed to continue to operate after spall initiation, the spall propagates, typically along the rolling direction, growing in size. A material with slow spall propagation rate is desirable as this increases the probability that the bearing failure can be detected before catastrophic failure. If a material has a high spall propagation rate, there is increased probability of catastrophic bearing failure, likely resulting in an engine in-flight shutdown and possible loss of aircraft. Some of the factors believed to influence spall propagation rate in bearings include material and heat treatment, operating conditions of load, speed, temperature, and lubricant, and accumulated subsurface damage caused by cyclic rolling contact stressing during bearing operation.

Rosado et al. [1], Mason et al. [2], and Trivedi et al. [3] have experimentally studied the spall propagation characteristics of relevant aerospace bearing materials. Additionally, microstructural and analytical studies of these materials have also been reported by Forster et al. [4], Arakere et al. [5], Branch et al. [6], Bhattacharya et al. [7], Pandkar et al. [8] and Kirsch et al. [9]. The present study builds from these investigations and focuses on spall propagation characteristics of bearings that have undergone long-term cyclic rolling contact stressing in a controlled laboratory environment. In applications, bearings may undergo billions of stress cycles before being removed from service due to failure by fatigue spall or other reasons (corrosion, lack of lubrication, pitting from contamination, reaching design life, etc.). During operation, the bearing material may undergo alteration in microstructure and residual stress. Alteration in microstructure of bearing steels from rolling contact is well documented in the literature, mostly on AISI 52100 steel (Swahn et al. [10], Voskamp [11, 12], Arakere [13]). These studies, together with those highlighted above, show that material transformation is a function of the number of stress cycles, operating temperature and load. It is widely believed that material transformation occurs due to the decay of austenite and martensite, the redistribution and generation of residual stresses, and change in hardness. These changes occur in a small material volume in the region of maximum shear and/or maximum von Mises stress below the surface. The analysis of this region for residual stress, retained austenite and micro-hardness have shown three stages of microstructural changes during rolling contact. These three stages involve: 1. Shakedown: initial micro-plastic flow and work hardening, 2. Steady state: micro- plastic flow, formation of dark etching regions (DER), white etching regions (WER) and white etching bands (WEB), and 3. Instability: buildup of residual stress, decrease in yield stress, and white etching crack (WEC) formation, with resultant increase in probability of fatigue spallation. The time required to go through these three stages can be significantly different based on alloying elements and heat treatment. Kirsch et al. [9] has shown that under accelerated test conditions, the density of white etching areas (WEA) in P675 bearing alloy was significantly lower compared to M50 and M50NiL. It is believed that the lower amount of material decay observed in P675 was likely attributed to its high alloy content and heat treatment resulting in a large number of suspensions and superior L_{10} fatigue life.

The primary objective of this study was to determine the effects of accumulated stress cycles on spall propagation time of through hardened AISI M50 and case carburized P675 bearing steels. Based on studies conducted on AISI 52100 noted above [10-12], the hypothesis was that bearings

with a higher number of accumulated stress cycles would have more subsurface material decay, hence shorter spall propagation life. The secondary objective was to study the difference in spall propagation time between bearings with natural fatigue spalls and spalls initiated from seeded faults, i.e., Rockwell C indentations on similarly life-tested bearings with the same number of accumulated stress cycles.

2 EXPERIMENTAL

2.1 Test Bearing Materials

The bearings evaluated in this study were 208-size angular contact bearings (40 mm bore) manufactured to ABEC 5 aerospace quality standards with outer land guided cages and split inner rings. The bearings were manufactured to a custom internal geometry per Table 1. The inner and outer rings were made from either VIM-VAR AISI M50 (AMS6491E) or VIM-VAR Pyrowear 675 (AMS5930A) steels. The M50 bearings were triple tempered at 540 °C and run in both an all-metal configuration with M50 rolling elements and in a hybrid configuration with silicon nitride ceramic rolling elements. P675, tested only in the hybrid configuration with silicon nitride rolling elements, was evaluated in both a low temperature temper (LTT) and a high temperature temper (HTT) condition. Both versions were double tempered at either 316 °C or 496 °C, respectively. The two heat treatment conditions of P675 are identified as P675 (LTT) and P675 (HTT).

All bearings were life tested at a constant thrust load of 22.25 kN resulting in a maximum Hertzian stress of 3.5 GPa for hybrid bearings and a maximum Hertzian stress of 3.1 GPa for all-metal bearings. The outer race temperature for all tests was held at 128 °C. The life testing procedure and results are described in detail in Reference 14. The life-tested bearings that were selected for spall propagation are listed in Tables 2 through 5. Life-tested bearings were all tested in pairs. When one bearing failed by fatigue spall, the other bearing was treated as a suspension. This resulted in pairs of bearings with identical run times/number of stress cycles and subjected to identical test conditions. For failed bearings, the naturally occurring fatigue spall was used as the starting point for spall propagation investigations. Conversely, suspended bearings were indented with seeded faults using Rockwell C indentations and subsequently run to initiate a fatigue spall prior to spall propagation. The spall initiation procedure for suspended bearings is described in detail in the following section. The spall propagation times for life-tested bearings were compared to new bearings. The "new bearing" spall propagation data used for comparison was extracted from References 3 and 14. Residual stress and limited retained austenite measurements were made as a function of depth in the hoop direction on the inner races using X-ray diffraction (XRD) in the ball track on selected life-tested bearings and compared to similar data obtained on as manufactured bearings. One life-tested inner race for each material pair was examined for microstructural changes. The life-tested inner races were cross sectioned along and across the rolling direction in order to examine the microstructure.

Table 1. Bearing Material and Geometry

Raceway material and	AISI VIM-VAR M50, Pyrowear 675
Ball material	Grade 10 AISI VIM-VAR M50, ABMA Grade 5 Toshiba TSN-03NH silicon nitride (Si_3N_4) balls
Cage material	Silver plated AISI 4340
Ball diameter, mm (in)	12.7 (0.5)
Number of balls	11
Pitch diameter, mm (in)	60.25 (2.37)
Bore diameter, mm (in)	40 (1.57)
Initial contact angle, deg	22

Table 2. List of Life Tested M50-M50 Bearings used for Spall Propagation

M50-M50		
Bearing #	**Stress Cycles (10^6)/Life (hr.)**	**Note**
357-A	6912.58/1804.9	Suspended
358	6912.58/1804.9	Spall
381	2933.51/765.9	Suspended
382	2933.51/765.9	Spall
379	1039.39/271.4	Spall
380	1039.39/271.4	Suspended
359	3261.47/851.6	Spall
360-A	3261.47/851.6	Suspended
357-B	5605.66/1463.6	Suspended
360-B	5605.66/1463.6	Spall

Table 3. List of Life Tested M50-Si_3N_4 Bearings used for Spall Propagation

M50 - Si_3N_4		
Bearing#	**Stress Cycles (10^6)/Life (hr.)**	**Note**
383	3779.10/986.7	Spall
384	3779.10/986.7	Suspended
385	2121.17/553.8	Suspended
386	2121.17/553.8	Spall
388	1150.72/300.5	Spall
399	665.58/173.8	Suspended
400	665.58/173.8	Spall
401	727.81/190	Suspended
402	727.81/190	Spall
443	5418.03/1414.6	Suspended
444	5418.03	Spall

Table 4. List of Life Tested P675 (LTT)-Si_3N_4 Bearings used for Spall Propagation

P675 (LTT)		
Bearing #	**Stress Cycles (10^6)/Life (hr.)**	**Note**
452	3206.44/837.2	Suspended
453	23719.46/6193.1	Suspended
454	23719.46/6193.1	Suspended
458	23611.95/6165	Suspended
460	4370.18/1141	Suspended
461	15623.64/4079.3	Spall
462	15623.64/4079.3	Suspended
467	1844.15/481.5	Suspended
469	12580.90/3284.8	Suspended
470	12580.90/3284.8	Suspended

Table 5. List of Life Tested P675 (HTT) - Si_3N_4 Bearings used for Spall Propagation

P675 (HTT)		
Bearing #	**Stress Cycles (10^6)/ Life (hr.)**	**Note**
583	19300.90/5039.4	Suspended
584	19300.90/5039.4	Suspended
586	19206.30/5014.7	Suspended
591	18845.13/4920.4	Spall
592	18845.13/4920.1	Suspended
593	19154.60/5001.2	Suspended

2.2 Test Rig and Procedure

The test rig used for spall initiation and propagation is shown in Figure 1. The test rig is designed to test 208-size (40 mm bore diameter) angular contact ball bearings. Each test head contains two 208-size test bearings mounted on a shaft separated by a spacer. For spall propagation on new bearings, a slave bearing was used in the back position. The position of life-tested bearings was either front or back during spall propagation tests to match the same position as used during life testing to maintain thrust load direction. The test shaft was rotated at 10,000 rpm by a 2.2 kW variable speed electric motor through a flexible coupling. The bearings were thrust loaded with the use of an adjustable hydraulic cylinder. No external radial load was applied. The bearings were lubricated with HTS turbine engine oil conforming to MIL-PRF-23699F supplied at a constant flow rate of 950 ml/min via two oil jets (one per bearing) using a recirculating lubrication system. The oil inlet temperature was maintained at 99 °C using oil tank heaters. The measured oil scavenge temperature was approximately 121 °C. The bearing test head was heated with electric resistance band heaters set to maintain the bearing outer race temperature at 128 °C. Additional details of the test rig are discussed in References 1 through 3 and 14.

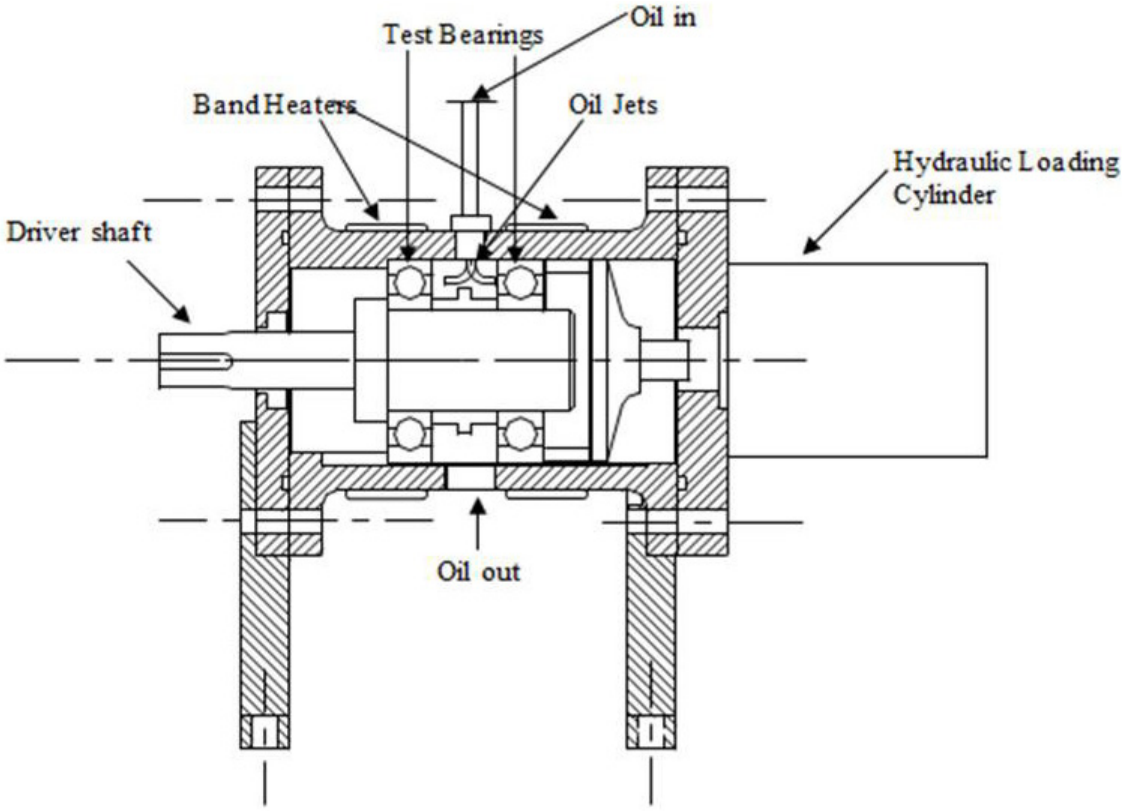

Figure 1. Bearing fatigue and spall propagation test rig schematic

Fatigue spalls were initiated through Rockwell C indents applied to suspended bearings. Hardness indents were placed on the bearing inner raceway surface to accelerate the spall initiation process. Rockwell C hardness indents are widely used to simulate bearing rolling contact fatigue life with contaminated oil and spall propagation performance tests [15-18]. Indents were placed manually using a Rockwell C indenter at a 150 kg load on a line oriented approximately 45 degrees across the ball track. Spall initiation tests from Rockwell C indents were conducted at a maximum Hertzian stress of 2.65 GPa (385 ksi) with an accelerometer vibration level set to 1 g. This level of vibration normally produced a fatigue spall similar to those that naturally resulted from fatigue life testing. A typical spall resulting from fatigue life testing and one initiated from Rockwell C indentations are shown in Figure 2. Spall propagation experiments were conducted under the same operating conditions as spall initiation, except the thrust load was lowered, resulting in a maximum Hertzian stress of 2.41 GPa (350 ksi). The mass loss resulting from spall progression was recorded using an in-line oil debris monitor (ODM) described in more detail in Refs. 1 through 3. The propagation test was stopped when the reported mass loss reached 1,000 mg. The bearing inner raceway was weighed and photographed at each stage of the test, after hardness indentations, spall initiation, and spall propagation.

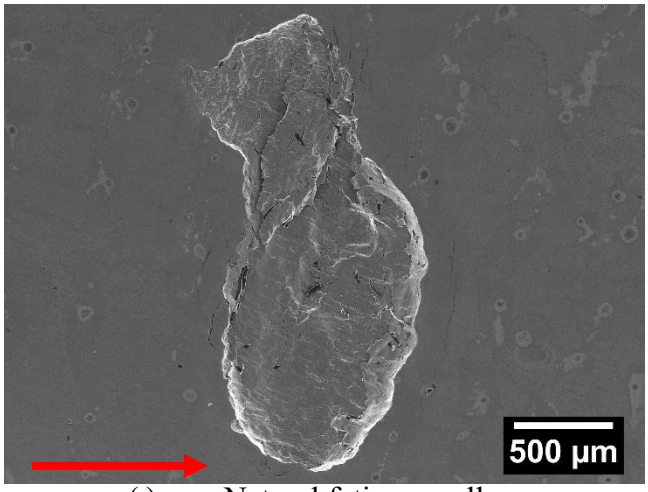

(a) Natural fatigue spall

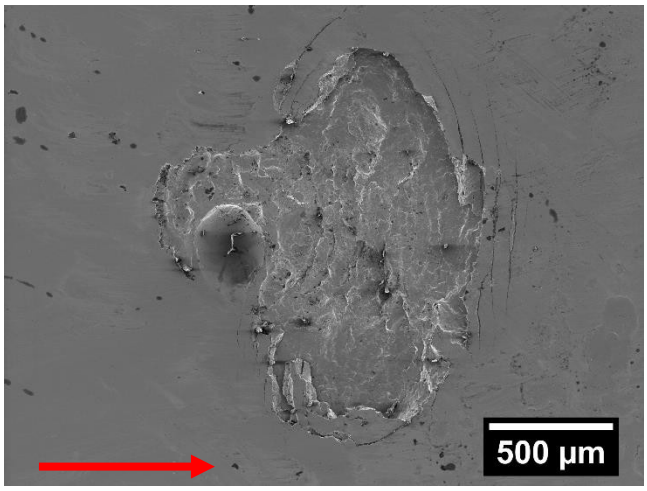

(b) Fatigue spall initiated from Rockwell C indentations

Figure 2. Spalls on bearing inner raceways

3 RESULTS AND DISCUSSION

The residual hoop stress as a function of depth for new and life tested bearing inner raceways is shown in Figure 3. All the materials have high surface residual stress resulting from final manufacturing processes. P675 is a case-carburized steel with a high compressive residual stress profile (~200 to 400 MPa) within the case (typical case depth is 1,000 to 1,250 micron) resulting from the carburizing process. All the life-tested material pairs analyzed for residual stress measurement were suspensions. The residual stress in the contact zone of life-tested bearings was increased significantly due to micro-plastic deformation/work hardening at a highly localized scale in subsurface volume (area of maximum shear stresses), resulting from repeated stress cycles. These results are similar to those observed in AISI 52100 by Voskamp [11-12]. Although the run times were different for the three hybrid materials, M50: 2,351 hours (9,004 x 10^6 stress cycles), P675 (LTT): 6,165 hours (23,612 x 10^6 stress cycles) and P675 (HTT): 5,001 hours (19,154 x 10^6 stress cycles), the maximum compressive residual stresses were similar (~700 MPa). However, the increase in compressive residual stress from the initial value was highest in M50 bearings. This suggest higher plastic micro-deformation in the M50 bearings, a result supported by the lower measured hardness of M50 relative to P675 [14]. Additionally, Klecka et al. [19] measured an approximate 8% decrease in compressive yield strength for thru-hardened M50 versus the P675 case material, increasing the likelihood of micro-plasticity for the same applied stress. This is further supported by WEBs developed in M50 bearings as shown in Figure 4. The volume of WEBs was much higher in the hybrid M50 bearing observed after shorter run time (9,004 x 10^6 stress cycles) compared to an all-metal M50 bearing (19,204 x 10^6 stress cycles). The increase in compressive residual stress and amount of WEB for all-metal M50 bearing were lower after 5,014 hours of testing due to lower maximum Hertzian stress of 3.1 GPa for the same applied thrust load. Swahn et al. [10] proposed that a carbon diffusion mechanism is responsible for formation of WEB. The density of WEB in hybrid M50 bearings is higher due to higher applied stress. The WEB was not observed in P675. The case carburized P675 has very high compressive residual stresses (~200 to 300 MPa), which lowers the Von Mises equivalent stress compared to M50 for the same applied Hertzian stress. It has been shown that for M50NiL with a compressive residual stress of 400 MPa, the Von Mises stress is reduced by 24% compared to M50 [20]. The reduction in Von Mises stress was found to be beneficial in reducing microstructural damage. The plastic micro-deformation in both P675 (LTT) and P675 (HTT) bearings was less compared to M50 bearings indicated by a smaller increase in compressive residual stress in P675. Only DER were observed in P675 bearings as shown in Figure 5. The formation DER has been identified as austenite/martensite decay [11]. There was a significant amount of retained austenite (RA) decay with P675 after 5,000 hours (19,000 x 10^6 stress cycles) as shown in Figure 6. The initial RA in VIM-VAR M50 was below 1% and the change in RA is believed to be very small, beyond the detection limit of XRD (Figure 6).

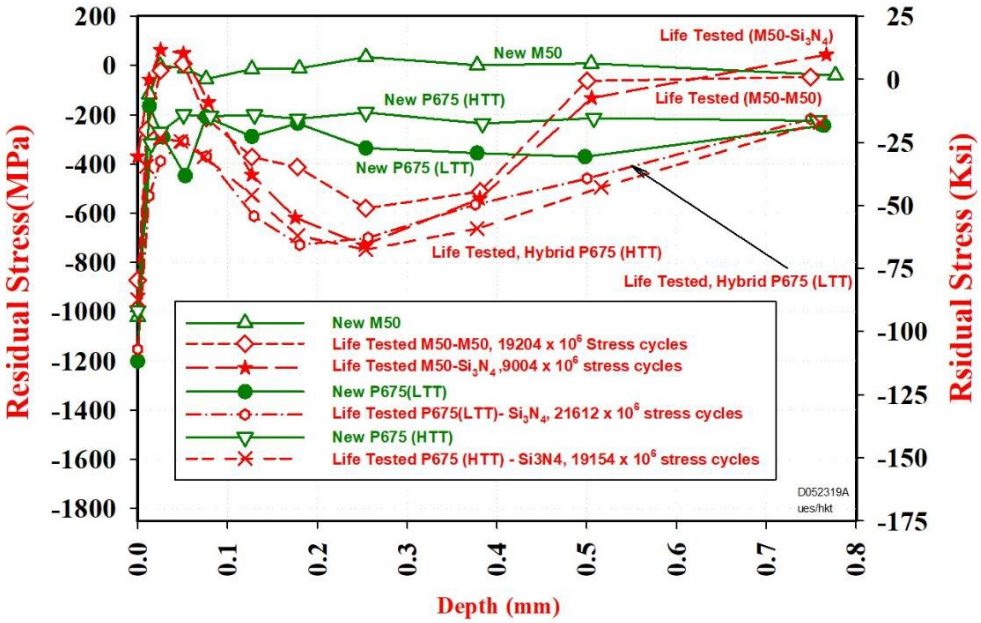

Figure 3. Comparison of residual stress between new and life tested bearing inner raceways

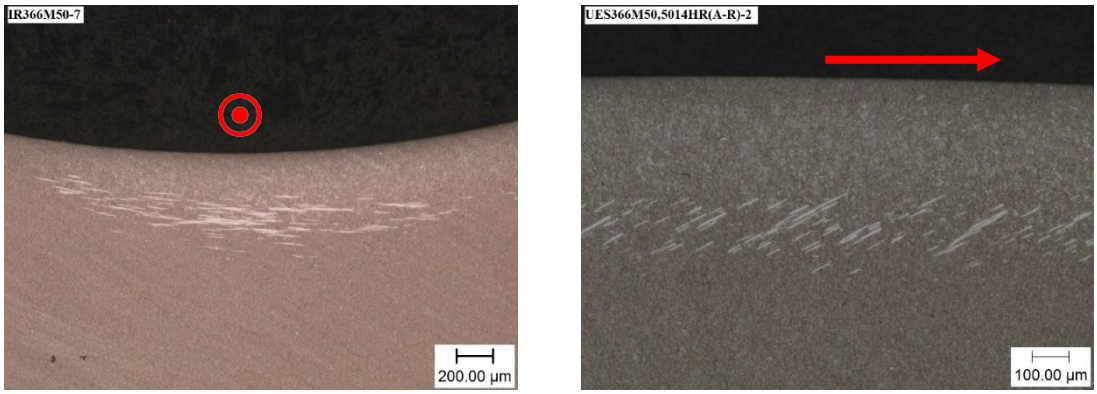

(a) M50-M50 Bearing, run time 5014 hours

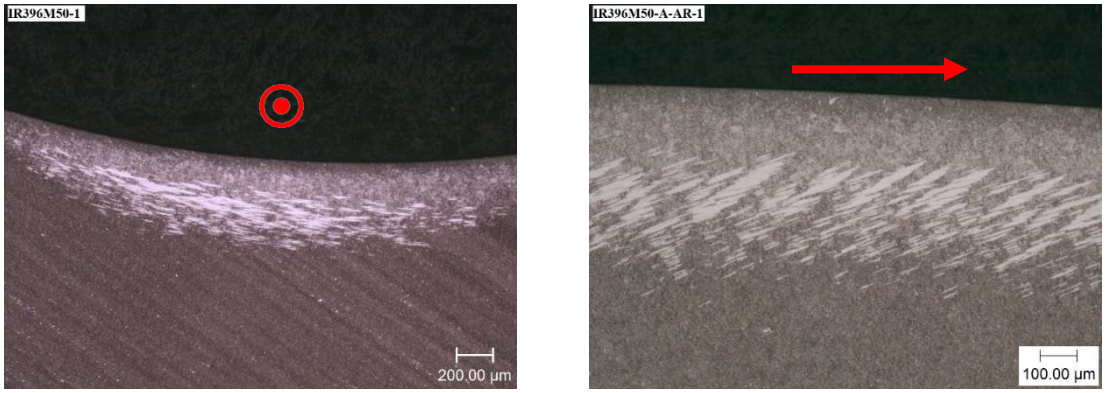

(b) M50-Si_3N_4 Bearing, run time 2351 hours

Figure 4. WEB developed on life tested M50 bearings

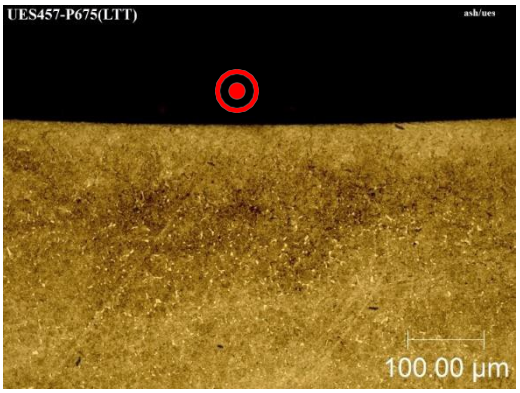

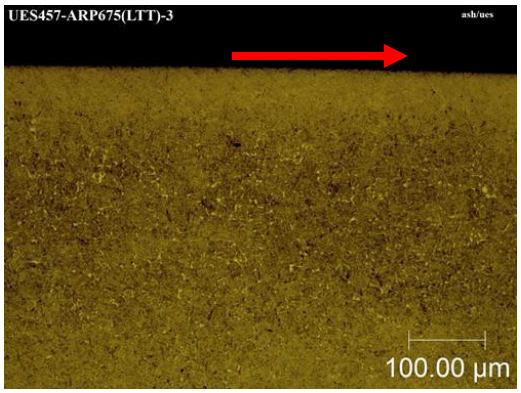

(a) P675 (LTT) – Si_3N_4 Bearing, run time 6165 hours

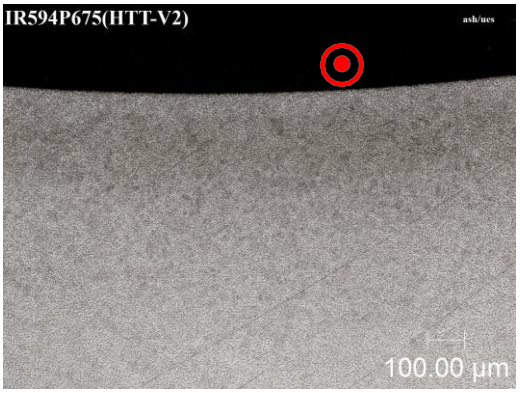

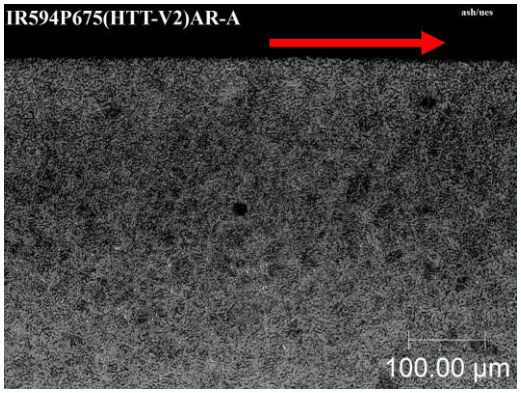

(b) P675 (HTT) – Si_3N_4 Bearing, run time 6165 hours

Figure 5. DER developed on life tested P675 bearings

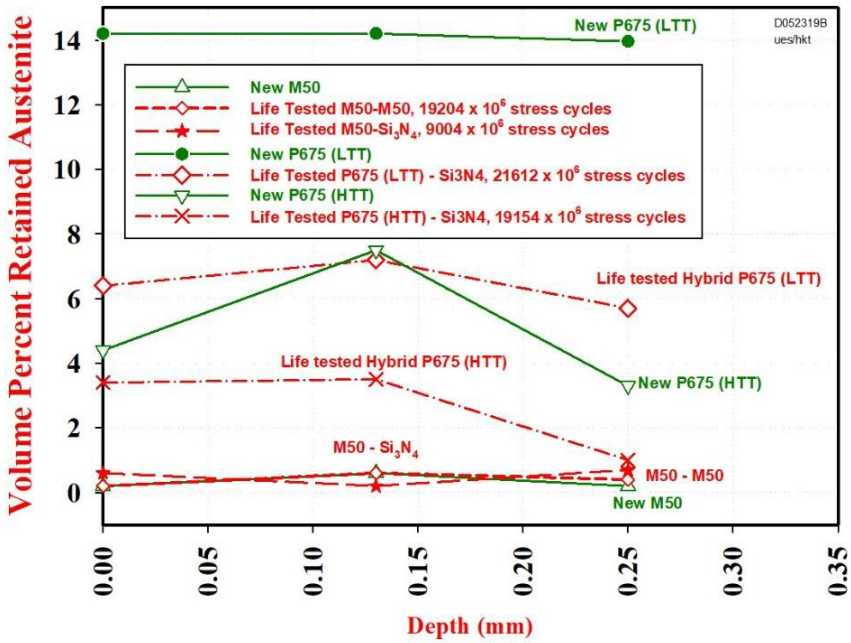

Figure 6. Comparison of retained austenite between new and stress cycles bearing

The spalls on suspended life-tested bearings were initiated using Rockwell C indentations. A majority of life-tested bearings for both tempers of P675 were suspensions with only one inner race failure by spallation (Tables 4 and 5). Conversely, approximately half of the M50 bearings failed by fatigue spall on the inner race regardless of rolling element material (Tables 2 and 3).

Figures 7 through 10 show the spall propagation trend plots for new and life-tested all-metal M50, hybrid M50, hybrid P675 (LTT) and hybrid P675 (HTT) as measured by the ODM. The tests were stopped when the mass loss reached 1,000 mg. The results were then calibrated using actual mass loss obtained by weighing the inner race. It is evident from the spall growth trend curves that both new and life-tested bearing materials typically exhibit an initial low-rate spall growth region followed by rapid critical growth or a "knee" in the curve. This mechanism is inherent to rolling contact fatigue spall growth and has been observed by Rosado et al. [1] and Mason et al. [2]. The spall propagation time to reach 100-mg actual mass loss was selected as the cut-off for all comparisons based on prior experience with 208-size bearings. It captures the spall propagation transition zone (from slow growth/incubation and propagation to accelerated propagation beyond the "knee" in the curve). The spall propagation times for 100 mg mass loss for new and life-tested bearings were analyzed using Analysis of Variance (ANOVA). Figure 11 shows comparisons of spall propagation time to 100 mg mass loss between new and life-tested bearings. Results for life-tested hybrid bearings is also summarized in Figure 12. In general, the mean spall propagation time to reach 100 mg mass loss for life-tested hybrid bearings (i.e., measure of spall propagation resistance) was: P675 (HTT) > P675 (LTT) > M50, with the most notable difference observed between P675 HTT and M50. There was no significant difference in spall propagation time between new and life-tested all-metal M50 bearings. However, there was a significant reduction in spall propagation time for life-tested hybrid M50 and hybrid P675 (LTT) bearings. Rosado et al. [1] reported similar observation for hybrid M50 bearings.

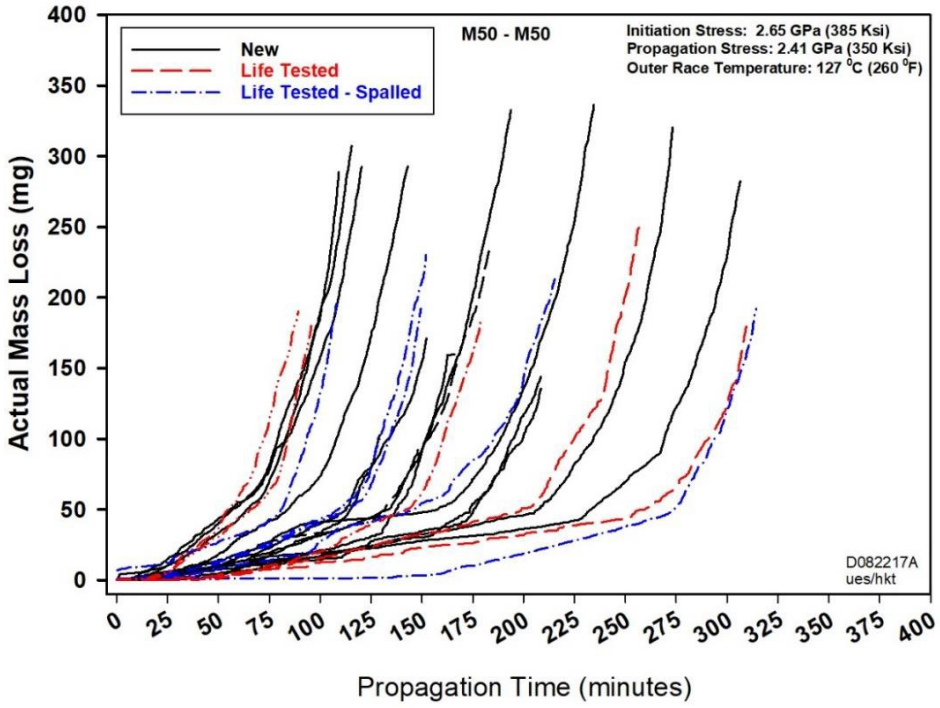

Figure 7. Spall propagation curves for new and life tested M50-M50 bearings

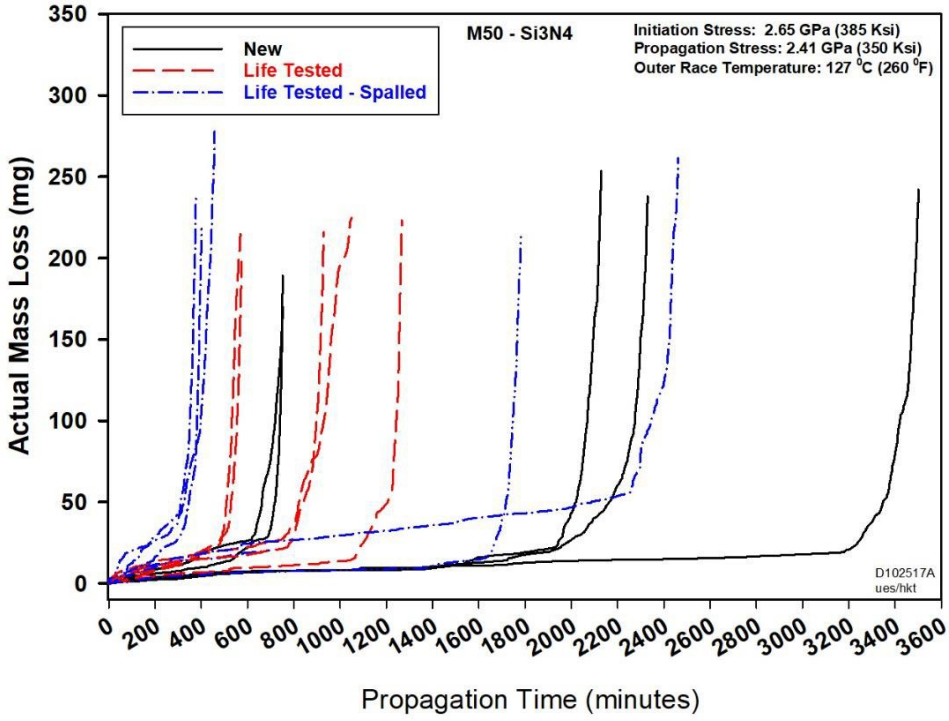

Figure 8. Spall propagation curves for new and life tested M50-Si_3N_4 bearings

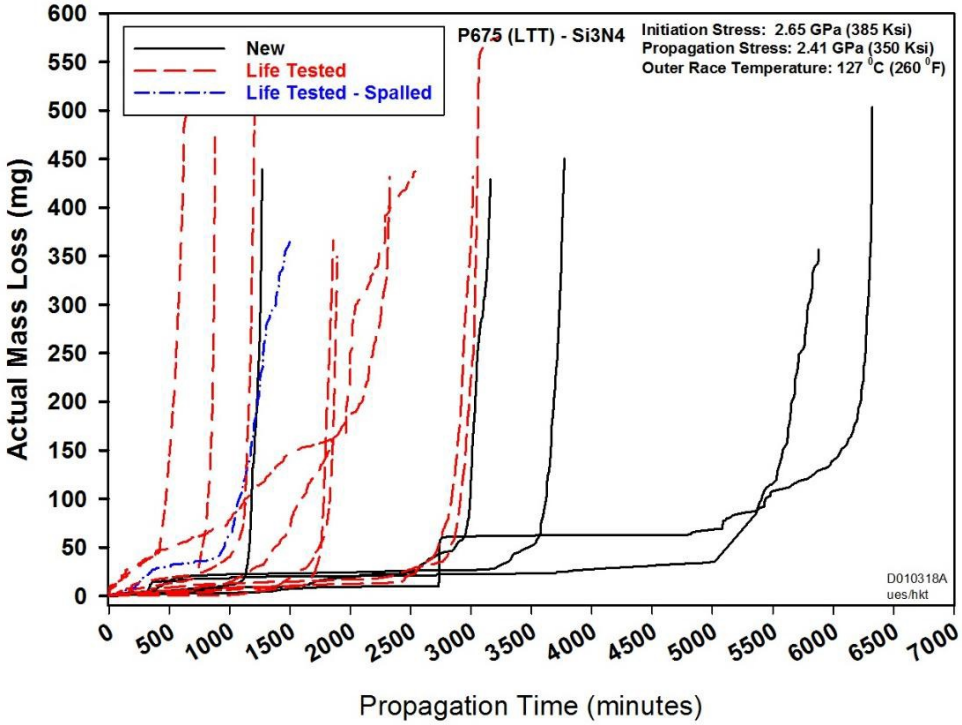

Figure 9. Spall propagation curves for new and life tested P675 (LTT)-Si_3N_4 bearings

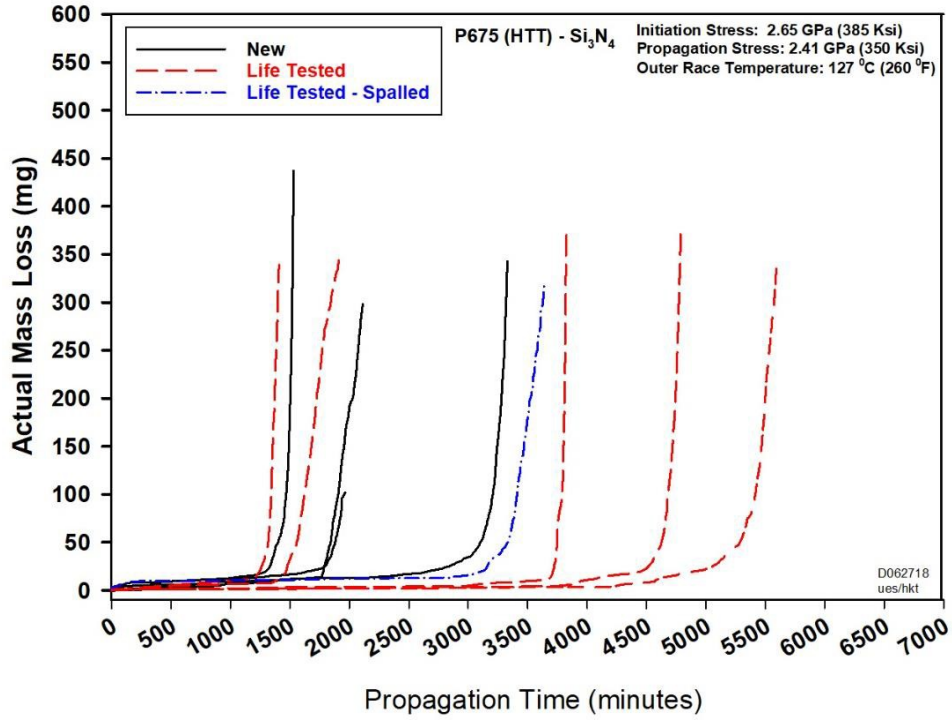

Figure 10. Spall propagation curves for new and life tested P675 (HTT)-Si_3N_4 bearings

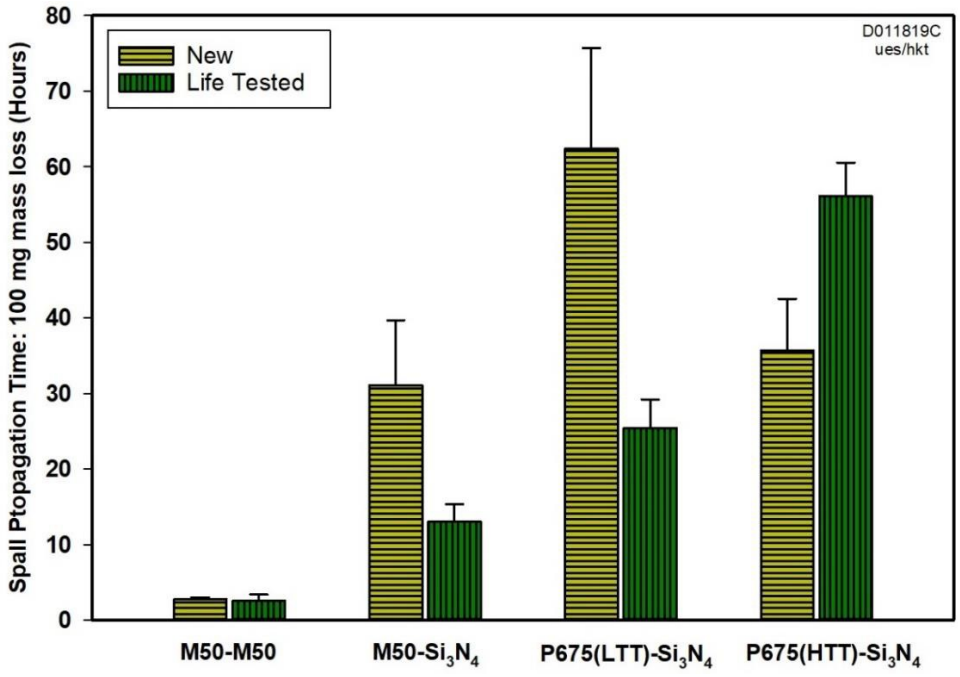

Figure 11. Comparison of spall propagation time (100 mg mass loss) between new and life tested bearings

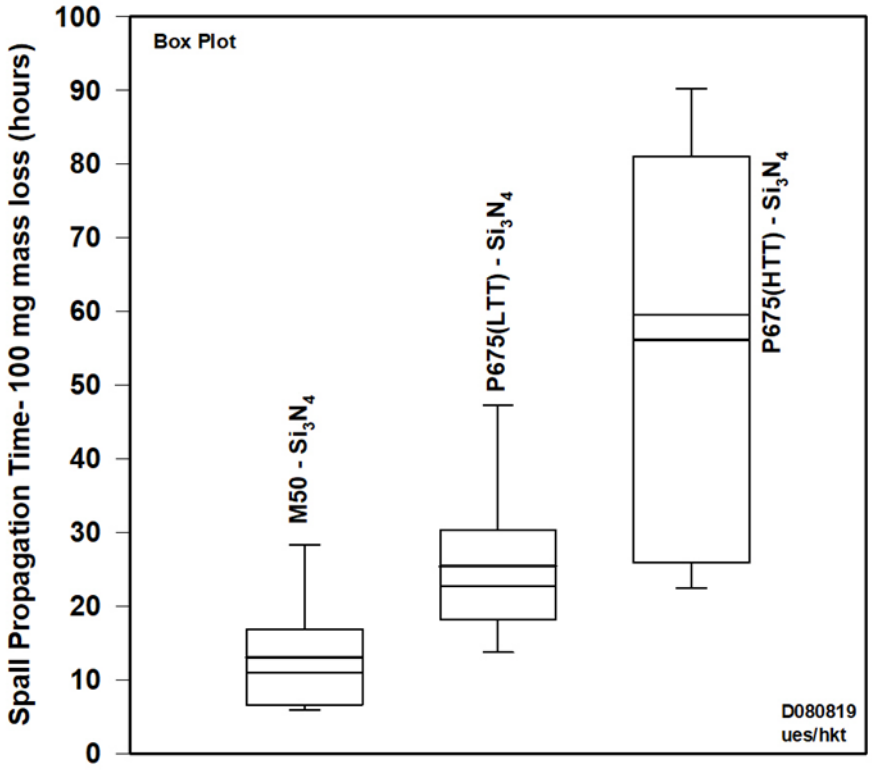

Figure 12. Comparison of spall propagation time (100 mg mass loss) between life-tested hybrid M50, P675 (LTT) and P675 (HTT) bearings

One possible key controlling factor for crack propagation is fracture toughness. It is likely the fracture toughness was reduced in the endurance tested bearings due to the transformation of retained austenite to martensite prior to spall propagation testing. The phenomenon of improved fracture toughness and enhanced RCF performance with the inclusion of retained austenite has been presented in literature and was reviewed recently by Sidoroff et al. [21] This loss in RA was especially prominent in the P675 (LTT) bearings, where the RA was reduced from an initial value of ~14% to ~6% after endurance testing (Figure 6). Since very little RA was present initially in M50, the loss of RA after endurance testing does not explain the difference in spall propagation times from the new condition. However, as noted earlier, a high density of material degradation in the form of DER and WEBs was observed in the hybrid M50 bearings after endurance testing. This transformation of material has been associated with a reduction in hardness. Specifically, Forster et al. [4] reported reduction in hardness (softening of material) in WEB region for a hybrid M50 bearing with 4,267 hours (16,343 x 10^6 stress cycles) of run time. It is believed that this reduction in hardness due to the formation of WEBs played a significant role in the loss of spall propagation performance.

Surprisingly, the life-tested hybrid P675 (HTT) bearings showed superior spall propagation times compared to new hybrid P675 (HTT) bearings. As discussed previously, significant compressive residual stresses were developed in the endurance tested bearings due to micro-plasticity within the contact. Since a high compressive residual stress has been shown by Trivedi et al. [3] to provide a substantial benefit in spall propagation resistance, it can be reasoned that this increased compressive stress after endurance testing should be beneficial. Since no WEBs were observed

in either P675 conditions, the controlling factors for spall propagation in this material appear to be a balance between the compressive stress field and the amount of remaining retained austenite present. Clearly, more testing and study is required to explain the disparity in spall propagation times between life-tested hybrid P675 (LTT) and P675 (HTT).

There was no significant difference in the ratio of reported to actual mass loss between new bearings and life-tested bearings as shown in Figure 13. Trivedi et al. [3] has shown that both bearing material and heat treatment have significant effects on the particle size generated during spall propagation. Both case carburized P675 tempers with silicon nitride rolling elements generated a larger number of smaller size particles compared to M50, in either the all-metal or hybrid configuration at 1,000 mg of reported mass loss. This is believed to be a result of the higher compressive residual stress in the case of the carburized materials. This higher compressive stress field acts to arrest the subsurface crack growth, as discussed earlier, and results in a shallower spall thereby producing smaller spall particles. Spall debris collected from various materials shows that the particles are generally flattened platelets. When calculating the mass loss from a given bearing, the ODM software assumes all particles to be spheres with diameters equal to some dimension of the passing particle. As the particle size increases so does the overestimation of mass loss since the volume contained within an equivalent diameter sphere grows relative to the flat discs. This was reflected in the resulting spall length as shown in Figure 14. ANOVA of spall lengths showed that the mean spall length for P675 was longer than M50 with a statistical significance. However, there was no significant difference in spall length between new and life-tested bearings. Trivedi et al. [3] showed that case carburized and nitrided material with silicon nitride rolling elements generated a larger number of smaller particles to reach 1,000 mg reported mass loss, resulting in longer spall lengths. This indicates that material decay from accumulated stress cycles has no effect on the size of particles and spall length.

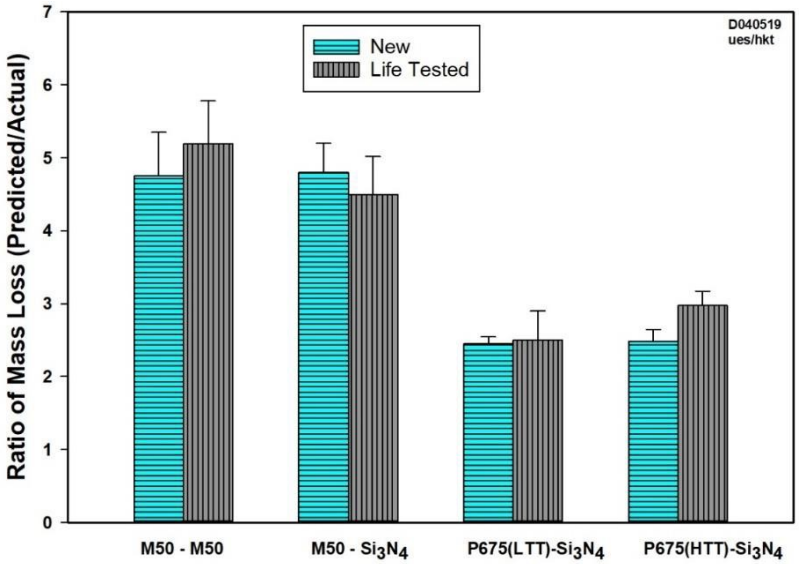

Figure 13. Comparison of mass loss ratio between new and life tested bearings

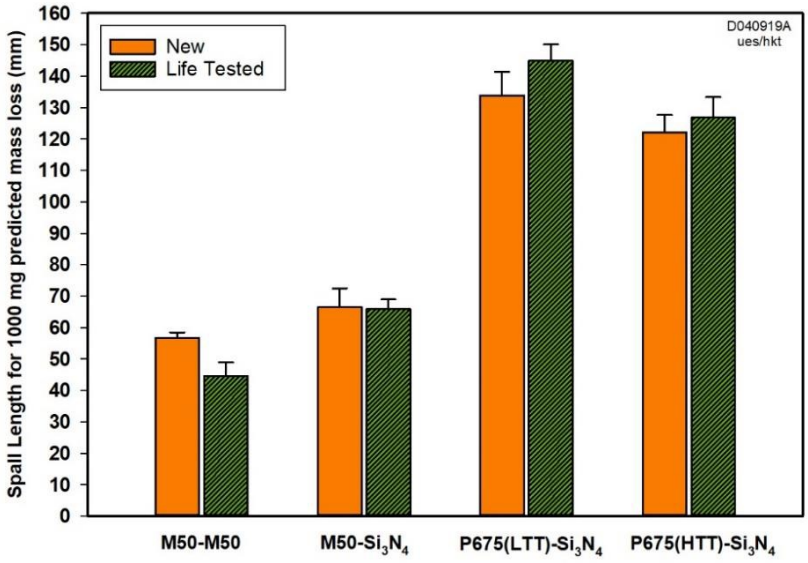

Figure 14. Comparison of spall length between new and life tested bearings

Swahn [10] and Voskamp [11] reported that in AISI 52100, the amount of material decay in the form of material transformation (DER, WEC), change in residual stress, and transformation of retained austenite increased with the number of stress cycles. Based on these two studies one can assume that bearings with longer run times will have a higher amount of material transformation, resulting in shorter spall propagation time. However, there was no direct quantitative correlation observed between accumulated run time and spall propagation time for M50 and P675 as shown in Figures 15 through 18. Additional testing and data would be needed to further study stress cycle-based material transformation trends in M50 and P675 and any associated effects on spall propagation rate.

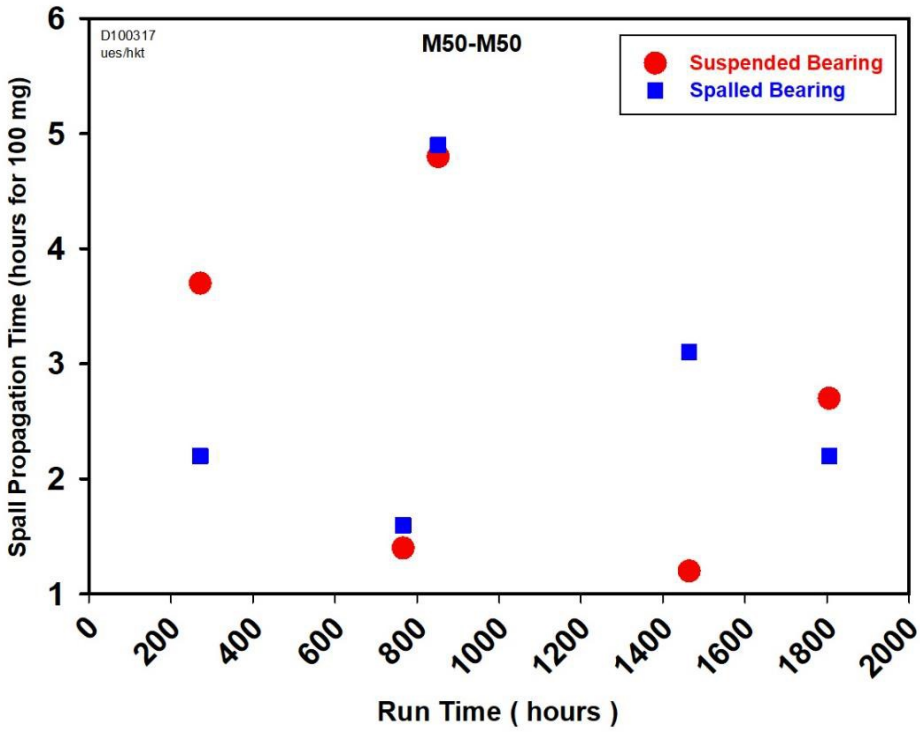

Figure 15. Relation between run time and spall propagation time for M50-M50 bearings

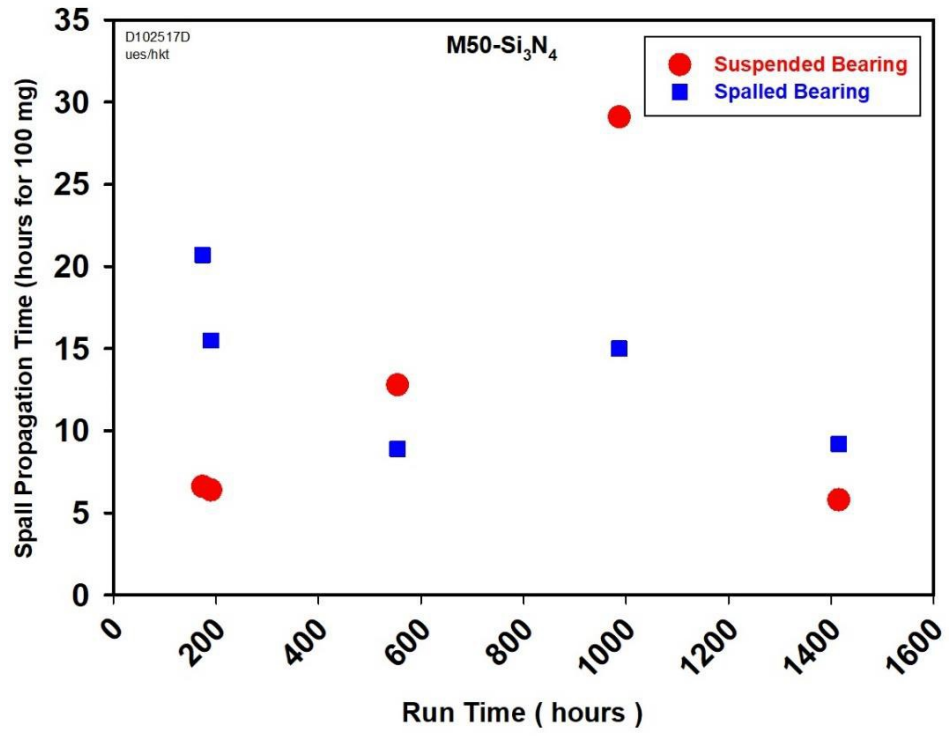

Figure 16. Relation between run time and spall propagation time for M50-Si_3N_4 bearings

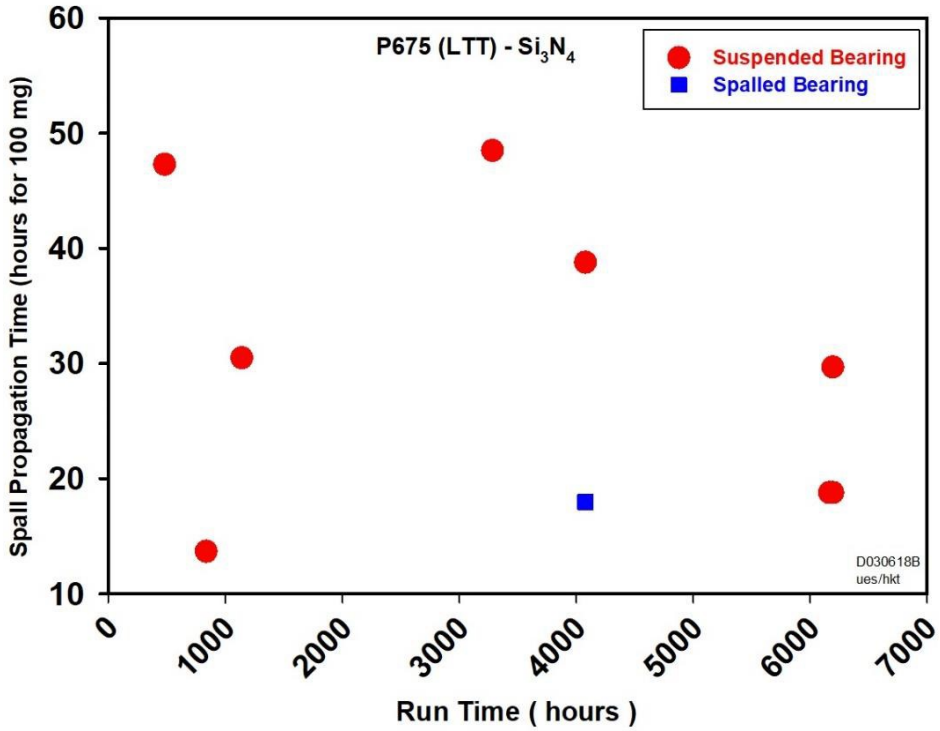

Figure 17. Relation between run time and spall propagation time for P675 (LTT)-Si_3N_4 bearings

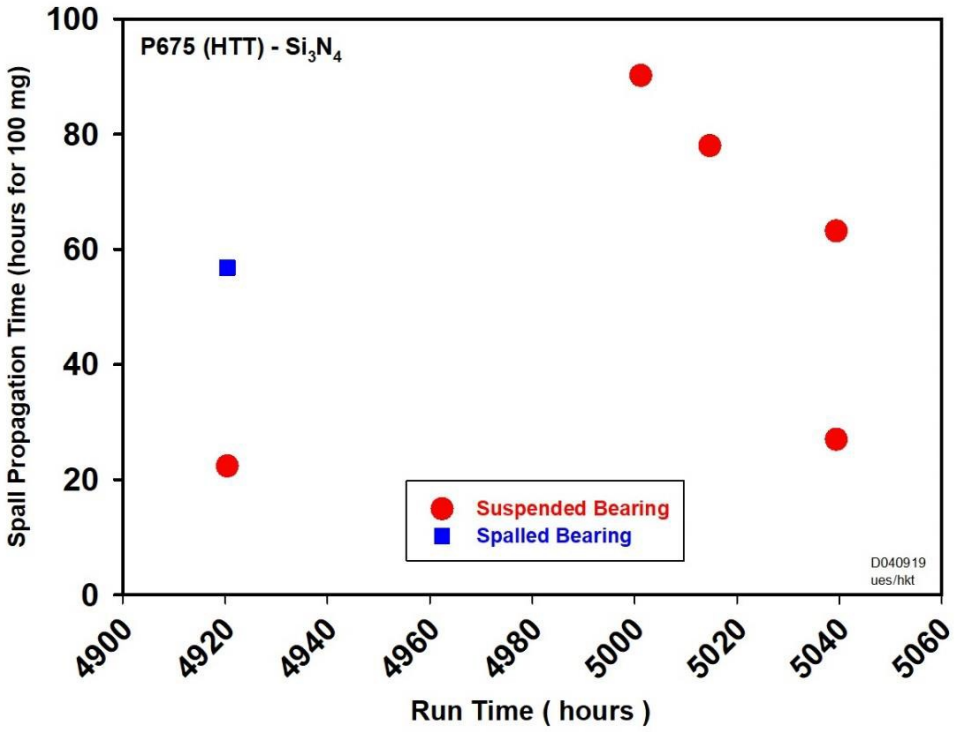

Figure 18. Relation between run time and spall propagation time for P675 (HTT)-Si_3N_4 bearings

The secondary objective was to study the difference in spall propagation time between natural fatigue spalls and spalls initiated from seeded Rockwell C indentations for life-tested bearings with a similar number of stress cycles. Based on the ANOVA results obtained with all-metal M50 and hybrid M50, there was no significant difference in spall propagation time observed for 100 mg mass loss between spalls propagated from Rockwell indents and spalls propagated from natural fatigue spalls. A box and whisker plot of mean spall propagation time to reach 100 mg mass loss for M50-M50 and M50-Si_3N_4 is shown in Figures 19 and 20, respectively. Only one spall propagation test was conducted from a natural fatigue spall on the inner raceway with both P675 (LTT) and P675 (HTT). Therefore, there was insufficient data to draw any conclusions on the effect of natural spalls versus spalls initiated from Rockwell C indents for these two materials.

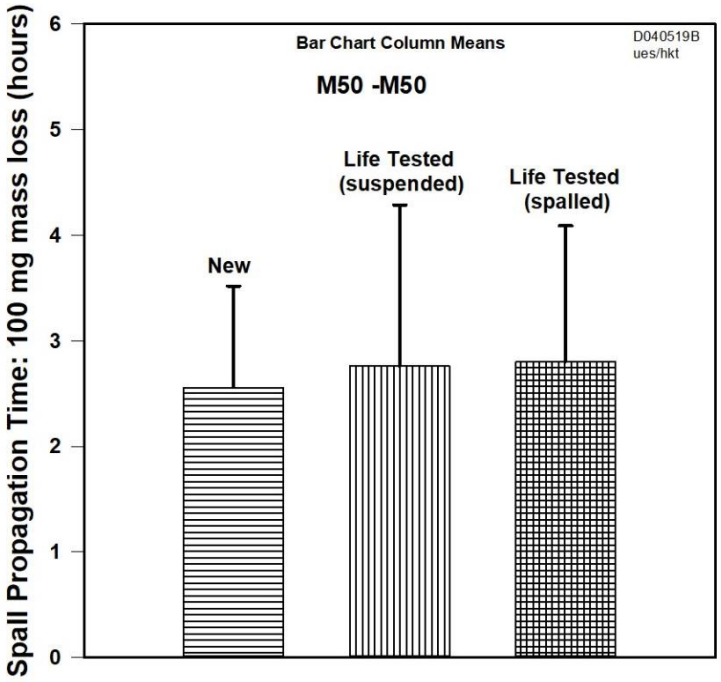

Figure 19. Comparison of spall propagation times for 100 mg mass loss between new and life tested M50-M50 bearings

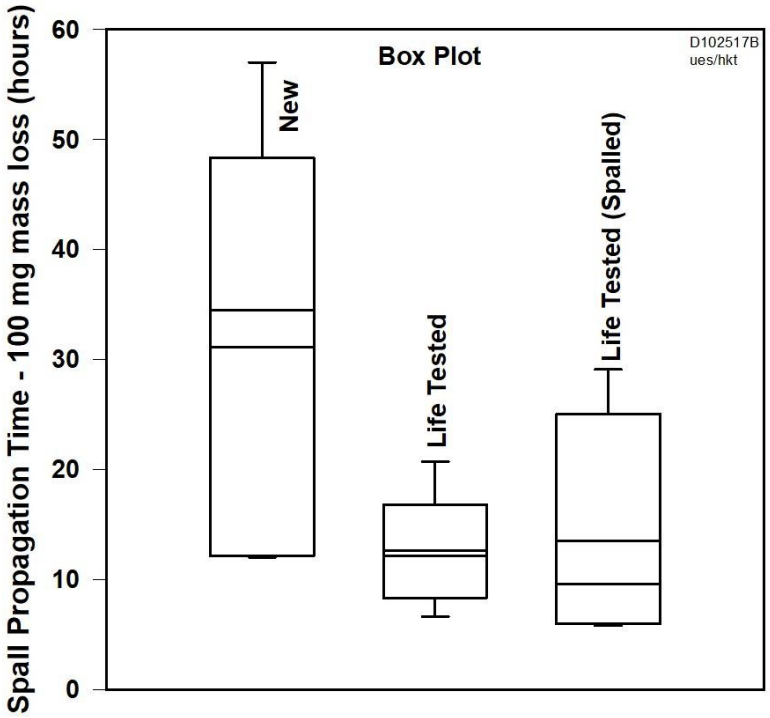

Figure 20. Box and Whisker plot for the mean response of all hybrid M50 bearing conditions on spall propagation time

4 CONCLUSIONS

The spall propagation characteristics of life-tested M50, Pyrowear 675 (LTT) and Pyrowear 675 (HTT) bearing steels was investigated and compared to "new bearing" data from a previous study. The results of this study are summarized below:

1. Subsurface material decay in the form of microstructural changes (WER/DER/WEA) and increased compressive residual stress was observed in all three life-tested materials. The amount of decay was much higher with through-hardened M50 compared to case carburized P675.
2. P675 materials generally exhibited longer spall propagation time over M50, with P675 (HTT) exhibiting a notable difference over M50.
3. No significant difference in spall propagation time was found between new and life-tested M50 all-metal bearings.
4. The accumulated stress cycles have a significant effect on spall propagation time (100 mg mass loss) for hybrid M50 and hybrid P675 (LTT) bearings. Life-tested hybrid M50 and P675 (LTT) bearings showed statistically significant lower spall propagation time compared to new bearings.
5. Life-tested hybrid P675 (HTT) bearings showed statistically longer spall propagation time compared to new hybrid P675 (HTT) bearings.
6. Based on M50 bearing test results, no difference in spall propagation time was observed between bearings with spalls initiated from seeded Rockwell C indents and those initiated from natural fatigue spalls.
7. Subsurface material microstructural decay/transformation caused by cyclic rolling contact stressing had a significant effect on spall propagation time.
8. No direct quantitative correlation was found however, between the accumulated run time or number of stress cycles and spall propagation time for life-tested bearings.

5 REFERENCES

1. Rosado, L., Forster, N.H, Thompson, K.L. and Cooke, J.W., "Rolling Contact Fatigue Life and Spall Propagation AISI M50, M50NiL, and AISI 52100, Part I: Experimental Results", Trib. Trans., Vol. 53, No. 1, pp 29-41, 2010.

2. Mason, J. K., Trivedi, H.K. and Rosado, L., "Spall Propagation Characteristics of Refurbished VIM-VAR M50 Angular Contact Ball Bearings", J. of Failure Analysis and Prevention, v17n3, March 2017, p. 426-439.

3. Trivedi, H.K., Haywood, D., Kirsch, M. S., and Rosado, L., "Spall Propagation Characteristics of as Manufactured Aerospace Bearing Steels", ASTM STP 1623, 2019

4. Forster, N.H., Rosado, L., Ogden, W.P. and Trivedi, H. K., "Rolling Contact Fatigue Life and Spall Propagation AISI M50, M50NiL, and AISI 52100, Part III: Metallurgical Examination", Trib. Trans., Vol. 53, No. 1, pp 52-59, 2010.

5. Arakere, N.K., Branch, N, Levesque, G., Svendsen, V .and Forster, N. H., "Rolling Contact Fatigue Life and Spall Propagation AISI M50, M50NiL, and AISI 52100, Part II: Stress Modeling", Trib. Trans., Vol. 53, No. 1, pp 42-51, 2010.

6. Branch, N.A., Arakere, N.K., Forster, N. and Svendsen, V., "Critical Stresses and Strains at the spall edge of a case hardened bearing due to ball impact", Int. J. of Fatigue, v47, 2013., p. 268-278.

7. Bhattacharya, A., Subhash, G., and Arakere, N., "Evaluation of Subsurface Plastic Zone due to Rolling Contact Fatigue of M50NiL case hardened Bearing Steel", Int. J. of Fatigue, 2014, Vol. 59, p.102-113.

8. Pandkar, A. S., Arakere, N., and Subhash, G., "Ratcheting-based Microstructure-sensitive modeling of the cyclic hardening response of case-hardened bearing steels subject to Rolling Contact Fatigue", Int. J. of Fatigue, 2015, Vol. 73, p. 119-131.

9. Kirsch, M. S. and Trivedi, H.K., "Microstructural Changes in Aerospace Bearing Steels under Accelerated Rolling Contact Fatigue Life testing", ASTM STP1600, 2017, p. 92-105.

10. Swahn, H., Becker, P.C. and Vigsbo, O., "Martensite Decay During Rolling Contact Fatigue in Ball Bearings", Metall. Trans. A, Vol. 7A, No. 9, 1976, p. 1976-1099.

11. Voskamp, A. P., "Microstructural Changes During Rolling Contact Fatigue", Ph.D. Thesis, 1997, Delft Univ. of Tech., Delft, The Netherlands.

12. Voskamp, A.P., "Fatigue and Material Response in Rolling Contact Fatigue", ASTM STP1327, 1998, p. 152-165.

13. Arakere, N. K., "Gigacycle rolling contact fatigue of bearing steels: A review", Int. J. of Fatigue, 2016, vol. 93, p. 238-249.

14. Trivedi, H. K., Rosado, L., Gerardi, D.T., Givan, G.D. and McCoy, B., “Fatigue Life Performance of Hybrid Angular Contact Pyrowear 675 Bearings”, ASTM STP1600, 2017, p. 275-295.

15. Girodin, D, Ville F., Guers, R. and Dundragne, G., “Rolling Contact Fatigue Tests to Investigate Surface Initiated Damage and Tolerance to Surface Dents”, ASTM STP 1419, 2002, p.263-281.

16. Streit, E., Brock J. and Poulin, P., “Performance Evaluation of Duplex Hardened Bearings for Advanced Turbine Engine Applications”, ASTM STP1465, 2007, p169-186.

17. Vincent, A., Nelias, D., Jacq, C., Robin, Y. and Dudragne, G., “Comparison of Fatigue Performance of 32CrMoV13 and M50 steels in Presence of Surface Dents”, ASTM STP1465, 2007, p 187-206.

18. Morales-Espejel, G.E. and Gabelli, A., “The Progression of Surface Rolling Contact Fatigue Damage of Rolling Bearings with Artificial Dents”, Trib. Tras., 58, (2015), p. 418-431.

19. Klecka, M.A., Subhash, G. and Arakere, N.H., “Microstructure-composition-property relationship in plastically graded case hardened steels”, Trib. Trans., 2013, V56, p. 1046-1059.

20. Forster, N.H., Peters, S. M., Chin, H.A., Poplawski, J.P. and Homan, R.J., “Applying Finite Element Analysis to Determine the subsurface Stress and Temperature Gradient in Highly Loaded Bearing Contracts”, ASTM STP1600, 2017, p.151-166.

21. Sindoroff, C., Perez, M, Dierickx, P. and Girodin, D., “Advantages and shortcomings of retained austenite in Bering steels: a review”, ASTM STP 1520, 2015, p.312-348.

LIST OF SYMBOLS, ABBREVIATIONS, AND ACRONYMS

ACRONYM	DESCRIPTION
ABMA	American Bearing Manufacturers Association
AFB	Air Force Base
AFRL	Air Force Research Laboratory
AISI	American Iron and Steel Institute
AMS	Aerospace Materials Specification
ANOVA	Analysis of Variance
DER	Dark Etching Region
HTS	High Thermal Stability
HTT	High Temperature Temper
LTT	Low Temperature Temper
ODM	Oil Debris Monitor
RA	Retained Austenite
RCF	Rolling Contact Fatigue
VAR	Vacuum Arc Remelting
VIM	Vacuum Induction Melting
WEA	White Etching Area
WEB	White Etching Band
WEC	White Etching Crack
XRD	X-ray Defraction